Extended optical model analyses of elastic scattering and fusion cross section data for the $^{12}C+^{208}Pb$ system at near-Coulomb-barrier energies by using a folding potential

W. Y. So[1,2] and T. Udagawa[1]
[1]*Department of Physics, University of Texas, Austin, Texas 78712, USA*
[2]*Department of Radiological Science, Catholic University of Pusan, Pusan 609-757, Korea*

S. W. Hong and B. T. Kim
Department of Physics and Institute of Basic Science, Sungkyunkwan University, Suwon 440-746, Korea
(Received 6 January 2008; published 29 February 2008)

Simultaneous χ^2 analyses are performed for elastic scattering and fusion cross section data for the $^{12}C+^{208}Pb$ system at near-Coulomb-barrier energies by using the extended optical model approach in which the polarization potential is decomposed into direct reaction (DR) and fusion parts. Use is made of the double folding potential as a bare potential. It is found that the experimental elastic scattering and fusion data are well reproduced without introducing any normalization factor for the double folding potential and also that both DR and fusion parts of the polarization potential determined from the χ^2 analyses satisfy separately the dispersion relation. Furthermore, it is shown that the imaginary parts of both DR and fusion potentials at the strong absorption radius change very rapidly, which results in a typical threshold anomaly in the total imaginary potential as observed with tightly bound projectiles such as α-particle and ^{16}O.

DOI: 10.1103/PhysRevC.77.024609 PACS number(s): 24.10.Ht, 25.70.Bc, 25.70.Jj

I. INTRODUCTION

Recently we carried out analyses [1–3] based on the extended optical model [4–6], in which the optical potential consists of the energy independent Hartree-Fock potential and the energy dependent complex polarization potential that has two components, i.e., the direct reaction (DR) and fusion parts, which we call the DR and fusion potentials, respectively. In the original work based on the extended optical model [4–6], use was made of a usual Woods-Saxon potential for the Hartree-Fock part of the potential, but in Refs. [1–3], we started using the double folding potential [7].

The main interest in the studies of Refs. [1–3] was the normalization constant N introduced earlier to reproduce the elastic scattering data for loosely bound projectiles such as ^{6}Li and ^{9}Be; in the analysis of data for such loosely bound projectiles using the usual optical model with a folding potential [7] one was forced to reduce the strength of the folding potential by a factor $N = 0.5 \sim 0.6$ in order to reproduce the data. This reduction factor was later ascribed to the strong breakup character of the projectiles. Studies were made on the effects of the breakup on the elastic scattering, based on the coupled discretized continuum channel (CDCC) method [8,9]. These studies were very successful in reproducing the elastic scattering data without introducing any arbitrary normalization factors and further in understanding the physical origin of the factor $N = 0.5 \sim 0.6$ needed in one channel optical model calculations. The authors of Refs. [8,9] projected their coupled channel equations to a single elastic channel equation and deduced the polarization potential arising from the coupling with the breakup channels. The resultant real part of the polarization potential was then found to be repulsive at the surface region around the strong absorption radius, R_{sa}. This means that the reduction of the folding potential by a factor of $N = 0.5 \sim 0.6$ needed in the one-channel optical model calculation is to effectively take into account the effects of the coupling with the breakup channels.

We explored this problem for the ^{6}Li [1], ^{7}Li [2] and ^{9}Be [3] induced scattering and fusion in the framework of the extended optical model with the double folding potential. Simultaneous χ^2 analyses of the elastic scattering and fusion cross section data were performed to determine the two types of the polarization potentials as functions of the incident energy $E_{\rm lab}$. Our expectation was that the resulting real part of the DR potential would become repulsive consistently with the results of the CCDC calculations. We have indeed obtained repulsive real DR polarization potentials [1–3]. In addition, it was shown that both DR and fusion potentials satisfied the dispersion relation [10,11] separately.

In the present study, we extend the work of Refs. [1–3] to the $^{12}C+^{208}Pb$ system. Since ^{12}C is a tightly bound projectile, such an anomalous normalization constant $N = 0.5 \sim 0.6$ observed in ^{6}Li or ^{9}Be induced scattering is not expected around the Coulomb barrier energies. In fact, the normalization factor N for reproducing the ^{12}C projectile data was found to be close to unity, $N \approx 1$ (see Ref. [7]).

In Sec. II, we first discuss characteristic features of elastic scattering cross section data of $^{12}C+^{208}Pb$ [12] in comparison with those of ^{6}Li induced scattering. From this comparison it will be shown that the DR cross section is expected to be significantly smaller in $^{12}C+^{208}Pb$ than in ^{6}Li or ^{9}Be induced reactions. In Sec. III, we then generate the so-called semi-experimental DR cross section, $\sigma_D^{\rm semi-exp}$, by using the elastic scattering data together with the fusion cross section data [13] by following the method described in, e.g., Ref. [14]. The data of $\sigma_D^{\rm semi-exp}$ is needed in making the separate determination of the DR and fusion potentials in the extended optical model. Simultaneous χ^2 analyses of the data of the elastic scattering, fusion and semi-experimental DR cross sections are then carried out in Sec. IV, where the results are also presented. Section V concludes the paper.

II. REVIEW OF EXPERIMENTAL CROSS SECTIONS

We begin with the discussion of some characteristic features of the elastic scattering cross section $d\sigma_{el}/d\sigma_\Omega$ data of ^{12}C+^{208}Pb in comparison with those of ^{6}Li, ^{7}Li, and ^{9}Be induced scattering [1–3]. Such features can best be seen in the ratio, P_E, defined by

$$P_E \equiv \frac{d\sigma_{el}}{d\sigma_\Omega} \Big/ \frac{d\sigma_C}{d\sigma_\Omega} = d\sigma_{el}/d\sigma_C \tag{1}$$

as a function of the distance of the closest approach D (or the reduced distance d), where $d\sigma_C/d\sigma_\Omega$ is the Coulomb scattering cross section, while D (d) is related to the scattering angle θ by

$$D = d\left(A_1^{1/3} + A_2^{1/3}\right) = \frac{1}{2} D_0 \left(1 + \frac{1}{\sin(\theta/2)}\right) \tag{2}$$

with

$$D_0 = \frac{Z_1 Z_2 e^2}{E} \tag{3}$$

being the distance of the closest approach in a head-on collision. Here (A_1, Z_1) and (A_2, Z_2) are the mass and charge of the projectile and target ions, respectively, and $E \equiv E_{\text{c.m.}}$ is the incident energy in the center-of-mass system. P_E as defined by Eq. (1) will be referred to as the elastic probability.

In Figs. 1(a) and 1(b), we present the experimental values of P_E for incident energies available around the Coulomb barrier energy as a function of the reduced distance d for ^{12}C+^{208}Pb

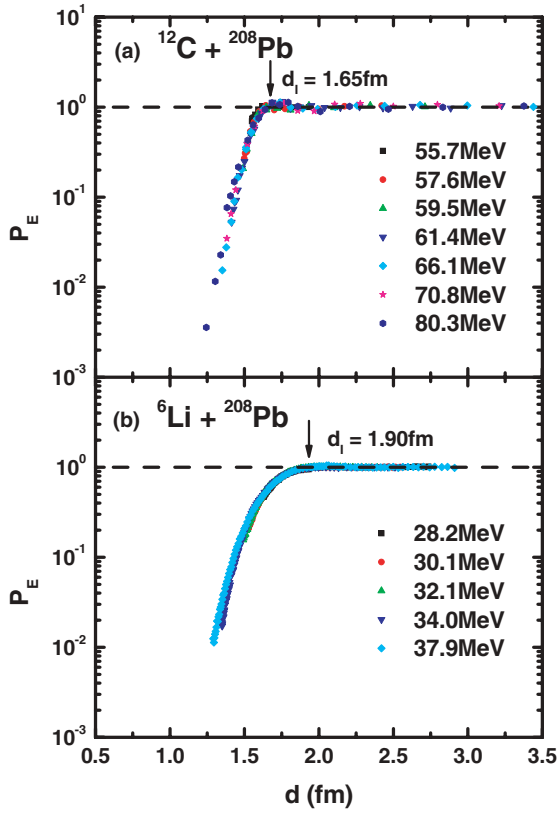

FIG. 1. (Color online) P_E values for the (a) ^{12}C+^{208}Pb system and (b) ^{6}Li+^{208}Pb system.

[13] and ^{6}Li+^{208}Pb [15] systems, respectively. The latter case is presented as an example of P_E for a loosely bound projectile. As seen, the values of P_E at different energies line up to form a very narrow band for both cases. This is a characteristic feature observed in many of the heavy-ion collisions, reflecting the semiclassical nature of the collisions. P_E remains close to unity until the two ions approach each other at around $d \sim d_I$, where P_E begins to fall off. The distance d_I is usually called the interaction distance, at which the nuclear interactions between the colliding ions are switched on, so to speak. The values of d_I are about 1.65 fm for ^{12}C+^{208}Pb and 1.9 fm for ^{6}Li+^{208}Pb.

The fall off of the P_E value in the region immediately next to d_I is due to DR. The fact that the d_I-value of 1.9 fm for ^{6}Li+^{208}Pb is much larger than $d_I = 1.65$ fm for ^{12}C+^{208}Pb implies that DR starts to take place in ^{6}Li+^{208}Pb at larger distances than it does in ^{12}C+^{208}Pb. Further it is seen that the amount of decrease of the P_E value from unity in ^{6}Li+^{208}Pb is significantly larger than in ^{12}C+^{208}Pb in the region of $d = 1.5 \sim 1.9$ fm, where DR takes place. These features clearly indicate that DR (which may be dominated by breakup) takes place significantly more strongly in ^{6}Li+^{208}Pb than in ^{12}C+^{208}Pb. This is indeed the case as seen from the semi-experimental DR cross section extracted in the next section.

Finally, we note that in the region of $d < 1.5$ fm where fusion dominates, the values of P_E for ^{12}C+^{208}Pb and ^{6}Li+^{208}Pb become almost identical, implying that there may not be much difference in the absorption rates of both systems when these colliding nuclei approach each other as close as $d < 1.5$ fm. In fact, the P_E value becomes 0.1 for both cases at approximately $d = 1.43 \sim 1.44$ fm.

III. EXTRACTING SEMI-EXPERIMENTAL DR CROSS SECTION

For our purpose of determining the fusion and DR potentials separately, it is desirable to have the data of DR cross sections in addition to fusion and elastic scattering cross sections. For the ^{12}C+^{208}Pb system, however, no reliable data of the DR cross section are available, although some efforts have been devoted to measure the inelastic and transfer reaction cross sections [12]. Here, we thus generate the so-called semi-experimental DR cross section $\sigma_D^{\text{semi-exp}}$, following the method proposed in Ref. [14].

Our method to generate $\sigma_D^{\text{semi-exp}}$ resorts to the well-known empirical fact that the total reaction cross section σ_R calculated from the optical model fit to the available elastic scattering cross section data, $d\sigma_E^{\text{exp}}/d\Omega$, usually agrees well with the experimental σ_R, in spite of the well known ambiguities in the optical potential. Let us call σ_R thus generated the semi-experimental reaction cross section $\sigma_R^{\text{semi-exp}}$. Then, $\sigma_D^{\text{semi-exp}}$ can be generated by

$$\sigma_D^{\text{semi-exp}} = \sigma_R^{\text{semi-exp}} - \sigma_F^{\text{exp}}. \tag{4}$$

This approach seems to work even for loosely bound projectiles, as demonstrated by Kolata *et al.* [16] for the ^{6}He+^{209}Bi system.

Following Ref. [14], we first carry out rather simple optical model χ^2 analyses of elastic scattering data solely for the purpose of deducing $\sigma_R^{\text{semi-exp}}$. For these preliminary analyses, we assume the optical potential to be the sum of $V_0(r)+iW_I(r)$ and $U_1(r, E)$, where $V_0(r)$ is the real, energy independent bare folding potential discussed in Sec. IV B, $iW_I(r)$ is an energy independent short range imaginary potential discussed in Sec. IV A, and $U_1(r, E)$ is a Woods-Saxon type complex potential with common geometrical parameters for both real and imaginary parts. The elastic scattering data are then fitted with a fixed radius parameter r_1 for $U_1(r, E)$, treating, however, three other parameters, the real and the imaginary strength V_1 and W_1 and the diffuseness parameter a_1, as adjustable. The χ^2 fitting is done for three choices of the radius parameter; $r_1 = 1.3$, 1.4, and 1.5 fm. These different choices of the r_1-value are made to examine the dependence of the resulting $\sigma_R^{\text{semi-exp}}$ on the value of r_1.

As observed in Ref. [14], the values of $\sigma_R^{\text{semi-exp}}$ thus extracted for three different r_1 values agree with the average value of $\sigma_R^{\text{semi-exp}}$ within 3%, implying that $\sigma_R^{\text{semi-exp}}$ is determined without much ambiguity. We then identified the average values as the final values of $\sigma_R^{\text{semi-exp}}$. Using thus determined $\sigma_R^{\text{semi-exp}}$, we generated $\sigma_D^{\text{semi-exp}}$ by employing Eq. (4). The resultant values of $\sigma_R^{\text{semi-exp}}$ and $\sigma_D^{\text{semi-exp}}$ are presented in Table I, together with σ_F^{exp}. In Table I, given are also $\sigma_R^{\text{semi-exp}}$ determined in Ref. [12] from the optical model calculations. The two sets of $\sigma_R^{\text{semi-exp}}$ determined independently agree within 6% except for the lowest energy case of $E_{\text{c.m.}} = 55.7$ MeV where the discrepancy amounts to 25%. However, at this energy the value of the cross section is very small, and thus $\sigma_R^{\text{semi-exp}}$ determined from the elastic scattering data has a relatively large uncertainty.

As seen in Table I, σ_F^{exp} is much larger than $\sigma_D^{\text{semi-exp}}$, and $\sigma_R^{\text{semi-exp}}$ is dominated by σ_F^{exp}. This is quite in contrast to the case for the ^{6}Li+^{208}Pb system, where $\sigma_R^{\text{semi-exp}}$ is dominated by $\sigma_D^{\text{semi-exp}}$ (see Table I of Ref. [1]). To demonstrate differences, we present in Fig. 2 the ratio, R_F, defined by

$$R_F \equiv \left(\sigma_F^{\text{exp}}/\sigma_R^{\text{semi-exp}}\right) \times 100 \tag{5}$$

for both ^{12}C+^{208}Pb and ^{6}Li+^{208}+Pb systems as a function of $E_{\text{c.m.}} - V_B$, V_B being the Coulomb barrier height. It is seen that the R_F values for the ^{12}C+^{208}Pb system are larger than 50% at all the energies considered and become close to 100% at $E_{\text{c.m.}} < V_B$, while for the ^{6}Li+^{208}Pb system the R_F values are less than 50% everywhere and become close to zero at $E_{\text{c.m.}} < V_B$. For the ^{12}C+^{208}Pb system, the reaction is dominated by fusion, in particular near and below the Coulomb barrier energy.

TABLE I. Semi-experimental total reaction and DR cross sections for the ^{12}C+^{208}Pb system.

E_{lab} (MeV)	$E_{\text{c.m.}}$ (MeV)	σ_F^{exp} (mb)	$\sigma_D^{\text{semi-exp}}$ (mb)	$\sigma_R^{\text{semi-exp}}$ (mb)	$\sigma_R^{\text{semi-exp}}$ (mb)
58.9	55.7	14	1	15	20
60.9	57.6	85	57	142	136
62.9	59.5	189	111	300	286
64.9	61.4	291	129	420	429
69.9	66.1	520	179	699	715
74.9	70.8	718	241	959	969
84.9	80.3	1045	327	1371	1373

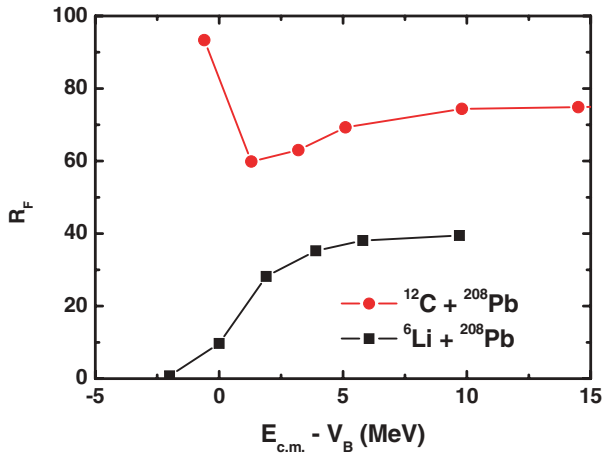

FIG. 2. (Color online) $R_F \equiv (\sigma_F^{\text{exp}}/\sigma_R^{\text{semi-exp}}) \times 100(\%)$ values for the ^{12}C+^{208}Pb and ^{6}Li+^{208}Pb systems.

IV. SIMULTANEOUS χ^2 ANALYSES

Simultaneous χ^2 analyses were then performed on the data sets of $(d\sigma_E^{\text{exp}}/d\Omega, \sigma_D^{\text{semi-exp}}, \sigma_F^{\text{exp}})$ by taking the data for $d\sigma_E^{\text{exp}}/d\Omega$, and σ_F^{exp} from the literature [12,13]. In calculating the χ^2 value, we simply assumed 1% errors for all the experimental data. The 1% error is about the average of errors in the measured elastic scattering cross sections, but much smaller than the errors in the DR (∼5%) and fusion (∼10%) cross sections. The choice of the 1% error for DR and fusion cross sections is thus equivalent to increasing the weight for the DR and fusion cross sections by factors of 25 and 100, respectively. Such a choice of errors may be reasonable, since we have only one datum point for each of these cross sections, while there are more than ten data points for the elastic scattering cross sections.

A. Necessary formulas

The optical potential $U(r, E)$ we use in the present work has the following form:

$$U(r; E) = V_C(r) - [V_0(r) + U_F(r; E) + U_D(r; E)], \tag{6}$$

where $V_C(r)$ is the usual Coulomb potential with $r_C = 1.25$ fm and $V_0(r)$ is the bare nuclear potential, for which use is made of the double folding potential described in the next subsection. $U_F(r; E)$ and $U_D(r; E)$ are, respectively, fusion and DR parts of the so-called polarization potential [17] that originates from couplings to the respective reaction channels. Both $U_F(r; E)$ and $U_D(r; E)$ are complex and their forms are assumed to be of volume-type and surface-derivative-type [5,18], respectively. $U_F(r; E)$, and $U_D(r; E)$ are explicitly given by

$$U_F(r; E) = (V_F(E) + iW_F(E))f(X_F) + iW_I(r), \tag{7}$$

and

$$U_D(r;E) = (V_D(E) + iW_D(E))4a_D \frac{df(X_D)}{dR_D}, \quad (8)$$

where $f(X_i) = [1+\exp(X_i)]^{-1}$ with $X_i = (r-R_i)/a_i (i = F$ and $D)$ is the usual Woods-Saxon function with the fixed geometrical parameters of $r_F = 1.40$ fm, $a_F = 0.35$ fm, $r_D = 1.50$ fm, and $a_D = 0.55$ fm, while $V_F(E)$, $V_D(E)$, $W_F(E)$, and $W_D(E)$ are the energy-dependent strength parameters. Since we assume the geometrical parameters of the real and imaginary potentials to be the same, the strength parameters $V_i(E)$ and $W_i(E)$ $(i = F$ or $D)$ are related through a dispersion relation [10],

$$V_i(E) = V_i(E_s) + \frac{E-E_s}{\pi} \mathrm{P} \int_0^\infty dE' \frac{W_i(E')}{(E'-E_s)(E'-E)}, \quad (9)$$

where P stands for the principal value and $V_i(E_s)$ is the value of $V_i(E)$ at a reference energy $E = E_s$. Later, we will use Eq. (9) to generate the final real strength parameters $V_F(E)$ and $V_D(E)$ using $W_F(E)$ and $W_D(E)$ fixed from χ^2 analyses.

The last imaginary potential $W_I(r)$ in $U_F(r;E)$ given by Eq. (7) is a short-range potential of the Woods-Saxon type given by

$$W_I(r) = W_I f(X_I), \quad (10)$$

with $W_I = 40$ MeV, $r_I = 1.0$ fm, and $a_I = 0.30$ fm. This imaginary potential is introduced to eliminate unphysical oscillations appearing in the radial wave functions of low partial waves when this $W_I(r)$ is not included. Because of the deep nature of the folding potential V_0 used in this study and also because $W_F(E)f(X_F)$, another imaginary part in $U_F(r;E)$, turns out to be not strong enough, reflections of lower partial waves appear, which causes the oscillations mentioned above, but physically such oscillations should not occur. $W_I(r)$ is introduced in order to eliminate this unphysical effect. We might introduce a real part $V_I(r)$ associated with $W_I(r)$, but we ignore this part, simply because such a real potential does not affect at all real physical observables, which means that it is impossible to extract the information of $V_I(r)$ from analyzing the experimental data.

In the extended optical model, fusion and DR cross sections, σ_F^{th} and σ_D^{th}, respectively, are calculated by using the following expression [4–6,19]:

$$\sigma_i^{\mathrm{th}} = \frac{2}{\hbar v} \langle \chi^{(+)} | \mathrm{Im}[U_i(r;E)] | \chi^{(+)} \rangle (i = F \text{ or } D), \quad (11)$$

where $\chi^{(+)}$ is the usual distorted wave function that satisfies the Schrödinger equation with the full optical model potential $U(r;E)$ in Eq. (6). σ_F^{th} and σ_D^{th} are thus calculated within the same framework as $d\sigma_E/d\Omega$ is calculated. Such a unified description enables us to evaluate all the different types of cross sections on the same footing.

B. The folding potential

The double folding potential $V_0(r)$ we use in the present study as the bare potential may be written as [7]

$$V_0(r) = \int d\mathbf{r}_1 \int d\mathbf{r}_2 \rho_1(r_1)\rho_2(r_2) v_{NN}(r_{12} = |\mathbf{r} - \mathbf{r}_1 + \mathbf{r}_2|), \quad (12)$$

where $\rho_1(r_1)$ and $\rho_2(r_2)$ are the nuclear matter distributions for the target and projectile nuclei, respectively, while v_{NN} is the M3Y interaction that describes the effective nucleon-nucleon interaction and the knock-on exchange effect given as

$$v_{NN}(r) = 7999 \frac{e^{-4r}}{4r} - 2134 \frac{e^{-2.5r}}{2.5r} - 262\delta(r). \quad (13)$$

For $\rho_1(r)$ we use the following Woods-Saxon form taken from Ref. [20]:

$$\rho_1(r) = \rho_0 \Big/ \left[1 + \exp\left(\frac{r-c}{z}\right)\right], \quad (14)$$

with $c = 6.624$ fm and $z = 0.549$ fm, while for $\rho_2(r)$ the following form is taken from Ref. [20]:

$$\rho_2(r) = \rho_0(1 + wr^2/c^2) \Big/ \left[1 + \exp\left(\frac{r-c}{z}\right)\right], \quad (15)$$

with $c = 2.355$ fm, $z = 0.522$ fm, and $w = -0.149$ fm. We then use the code DFPOT of Cook [21] for evaluating $V_0(r)$.

C. Threshold energies of sub-barrier fusion and DR

As in Ref. [1], we utilize as an important ingredient the so-called threshold energies $E_{0,F}$ and $E_{0,D}$ of sub-barrier fusion and DR, respectively, which are defined as zero intercepts of the linear representation of the quantities $S_i(E)$, defined by

$$S_i \equiv \sqrt{E\sigma_i} \approx \alpha_i (E - E_{0,i}) (i = F \text{ or } D), \quad (16)$$

where α_i is a constant. S_i with $i = F$, i.e., S_F is the quantity introduced originally by Stelson *et al.* [22], who showed that in the sub-barrier region S_F from the measured σ_F could be represented very well by a linear function of E (linear systematics) as in Eq. (16). In Ref. [18], we extended the linear systematics to DR cross sections. In fact the DR data are also well represented by a linear function.

In Fig. 3, we present the experimental $S_F(E)$ and $S_D(E)$. For $S_D(E)$, use is made of $\sigma_D^{\text{semi-exp}}$. From the zeros of $S_i(E)$, one can deduce $E_{0,D}^{\text{semi-exp}} = 55.6$ MeV and $E_{0,F}^{\text{exp}} = 53.7$ MeV. For both $i = F$ and D, the observed S_i are very well approximated by straight lines in the sub-barrier region and thus $E_{0,i}$ can be extracted without much ambiguity. $E_{0,D}^{\text{semi-exp}}$ is found to be about 2 MeV higher than $E_{0,F}^{\text{exp}}$, showing that the DR channels open at higher energies than fusion channels, which is somewhat unusual; normally the DR channels open at lower energies than fusion channels. This unusual opening of the DR channels at higher energies than fusion is related to the small DR cross sections at lower energies as shown in Table I and Fig. 2. The ^{12}C+^{208}Pb system is a system in which DR takes place very weakly particularly at lower energies.

$E_{0,i}$ may then be used as the energy where the imaginary potential $W_i(E)(i = F, D)$ in Eqs. (7) and (8) becomes zero,

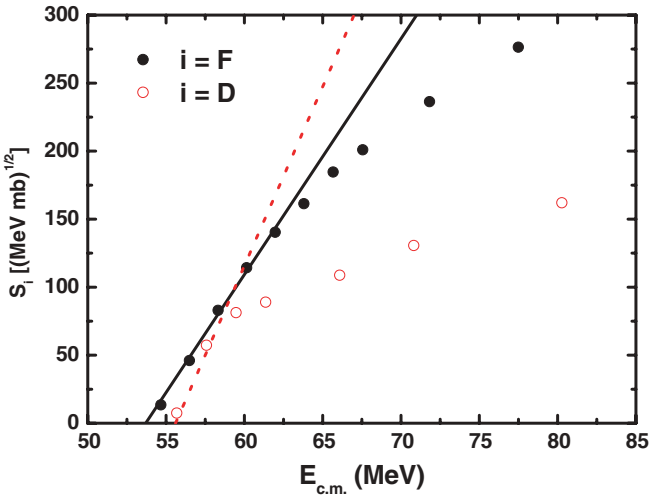

FIG. 3. (Color online) The Stelson plot of $S_i = \sqrt{E\sigma_i}$ for DR ($i = D$, open circles) and fusion ($i = F$, filled circles) cross sections. Use is made of the semi-experimental DR cross section for S_D, while the experimental fusion cross section is employed for S_F. The intercepts of the straight lines with the energy axis give us the threshold energies $E_{0,D}^{\text{semi-exp}} = 55.6$ MeV and $E_{0,F}^{\text{exp}} = 53.7$ MeV.

i.e., $W_i(E_{0,i}) = 0$ [18,23]. This procedure will be used in the next subsection for obtaining a mathematical expression for $W_i(E)$.

D. χ^2 analyses

All the χ^2 analyses performed in the present work are carried out by using the folding potential described in Sec. IV B as the bare potential $V_0(r)$ and by using the fixed geometrical parameters for the polarization potentials, $r_F = 1.40$ fm, $a_F = 0.35$ fm, $r_D = 1.50$ fm, and $a_D = 0.55$ fm, which are close to the values used in our previous study [18]. A slight change of the values from those of Ref. [18] was made to improve the χ^2 fitting.

As in Ref. [18], the χ^2 analyses are done in two steps; in the first step, all four strength parameters, $V_F(E)$, $W_F(E)$, $V_D(E)$ and $W_D(E)$ are varied. In this step, we can fix fairly well the strength parameters of the DR potential, $V_D(E)$ and $W_D(E)$, in the sense that $V_D(E)$ and $W_D(E)$ are determined as a smooth function of E. The values of $V_D(E)$ and $W_D(E)$ thus extracted are presented in Fig. 4 by open circles. The values of $W_D(E)$ thus extracted can be well represented by the following function of E (in units of MeV):

$$W_D(E) = \begin{cases} 0 & \text{for } E \leqslant E_{0,D}^{\text{semi-exp}} = 55.6 \\ 0.147(E - 55.6) & \text{for } 55.6 < E \leqslant 59.0 \\ 0.007(E - 59.0) + 0.15 & \text{for } 59.0 < E \leqslant 111.0 \\ 0.50 & \text{for } 111.0 < E \end{cases} . \quad (17)$$

Note that the threshold energy where $W_D(E)$ becomes zero is set equal to $E_{0,D}^{\text{semi-exp}}$ as determined in the previous subsection and are also indicated by the open circle at $E = 55.6$ MeV in Fig. 4. The dotted line in the lower panel of Fig. 4 represents

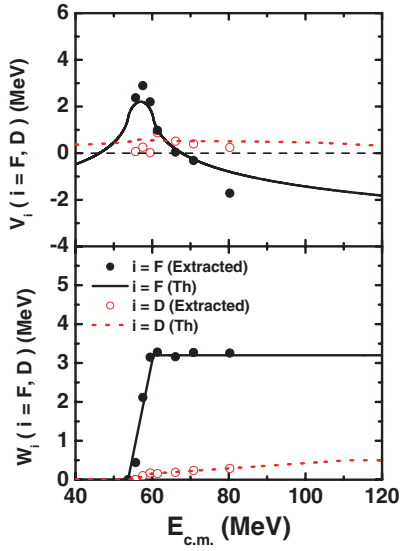

FIG. 4. (Color online) The strength parameters V_i (upper panel) and W_i (lower panel) for $i = D$ and F as functions of $E_{\text{c.m.}}$. The open and solid circles are the strength parameters for $i = D$ and F, respectively. The dotted and solid lines in the lower panel denote W_D and W_F from Eqs. (17) and (18), respectively, while the dotted and solid curves in the upper panel represent V_D and V_F calculated by using the dispersion relation of Eq. (9) with W_i given by Eqs. (17) and (18). The values of $V_i(E_s)$ and the corresponding reference energies E_s used in Eq. (9) are such that $V_F(E_s = 60.3\,\text{MeV}) = 1.5$ MeV and $V_D(E_s = 59.0\,\text{MeV}) = 0.57$ MeV, respectively.

Eq. (17). The dotted line in the upper panel of Fig. 4 denotes V_D as predicted by the dispersion relation of Eq. (9), with $W_D(E)$ given by Eq. (17). As seen, the dotted lines reproduce the open circles fairly well, indicating that $V_D(E)$ and $W_D(E)$ extracted by the χ^2 analyses satisfy the dispersion relation.

In this first procedure of the χ^2 fitting, however, the values of $V_F(E)$ and $W_F(E)$ are not reliably fixed in the sense that the extracted values fluctuate considerably as functions of E. This is understandable from the expectation that the elastic scattering can probe most accurately the optical potential in the peripheral region, which is nothing but the region characterized by the DR potential. The part of the nuclear potential responsible for fusion is thus difficult to pin down in this first step.

To obtain more reliable information on V_F and W_F, we thus performed the second step of the χ^2 analysis; this time, instead of doing a four-parameter search we fixed V_D and W_D as determined by the first χ^2 fitting, i.e., $W_D(E)$ given by Eq. (17) and $V_D(E)$ predicted from the dispersion relation. We then performed two-parameter χ^2 analyses, treating only $V_F(E)$ and $W_F(E)$ as adjustable parameters. The parameter values thus determined are presented in Fig. 4 by solid circles. The solid circles in the lower panel of Fig. 4 can be well represented by

$$W_F(E) = \begin{cases} 0 & \text{for } E \leqslant E_{0,F}^{\text{exp}} = 53.7 \\ 0.485(E - 53.7) & \text{for } 53.7 < E \leqslant 60.3 \\ 3.20 & \text{for } 60.3 < E \end{cases} . \quad (18)$$

As is done for $W_D(E)$, the threshold energy where $W_F(E)$ becomes zero is set equal to $E_{0,F}^{\rm exp}$ that is also indicated by the solid circle in Fig. 4. As seen, the $W_F(E)$ values determined by the second χ^2 analyses can fairly well be represented by the functions given by Eq. (18).

Using $W_F(E)$ given by Eq. (18), one can generate $V_F(E)$ from the dispersion relation. The resulting $V_F(r)$ is shown by the solid curve in the upper panel of Fig. 4, which again well reproduces the values extracted from the χ^2 fitting. This result shows that the fusion potential determined from the present analysis also satisfies the dispersion relation.

Note that the energy variations in $W_F(E)$ and $V_F(E)$ are more rapid compared to those in $W_D(E)$ and $V_D(E)$, and are similar to those in tightly bound projectiles [24–26]. It is thus seen that the resultant $V_F(E)$ and $W_F(E)$ exhibit the threshold anomaly.

E. Final calculated cross sections in comparison with the data

Using $W_D(E)$ given by Eq. (17) and $W_F(E)$ given by Eq. (18) together with $V_D(E)$ and $V_F(E)$ generated by the dispersion relation, we have performed the final calculations of the elastic, DR and fusion cross sections. The results are presented in Figs. 5 and 6 in comparison with the experimental data. All the data are well reproduced by the calculations.

It may be worth noting here that the theoretical fusion cross section, $\sigma_F^{\rm th}$, includes contributions from two imaginary components $W_I(r)$ and $W_F(r) = W_F(E) f(X_F)$ in $U_F(r, E)$ of Eq. (7). In Table II the partial contributions from $W_I(r)$ and $W_F(r)$, denoted by σ_I and σ_F, respectively, are presented separately, together with the total theoretical fusion cross section, $\sigma_F^{\rm th}$. As seen, the contribution from the inner part, $W_I(r)$, amounts to less than 10% except at highest energies $E_{\rm c.m.} = 80.3$ MeV, where the inner part contributes by 14%. This enhanced contribution from the inner part at higher energies may be due to deeper penetration of the projectile into the inner part at higher energies.

It should be recalled at this stage that we assumed a constant value of $W_I = 40$ MeV. Such an assumption is apparently inconsistent with a rapid energy variation expected to exist in the fusion potential around the Coulomb barrier energy. Note, however, that elastic scattering, fusion and total reaction cross sections are all rather insensitive to the value of $W_I(r)$, in particular, at low energies below the Coulomb barrier energy as discussed somewhat in details in Sec. IV B of Ref. [2]. Considering this and also the fact that $V_I(r)$, the real potential associated with $W_I(r)$, would also be insensitive to the observables, one could make the inner part of the imaginary fusion potential $W_I(r)$ to be fully dispersive and energy dependent. We have not tried here to make such an extension, since as emphasized earlier one cannot achieve it without ambiguity due to the fact that the observables cannot be reflective of the inner part of the potential.

TABLE II. Partial contributions σ_F and σ_I to the fusion cross sections.

$E_{\rm lab}$ (MeV)	$E_{\rm c.m.}$ (MeV)	σ_I (mb)	σ_F (mb)	$\sigma_F^{\rm th}$ (mb)
58.9	55.7	1	13	14
60.9	57.6	5	71	76
62.9	59.5	9	171	180
64.9	61.4	12	269	281
69.9	66.1	37	482	520
74.9	70.8	72	659	731
84.9	80.3	149	925	1073

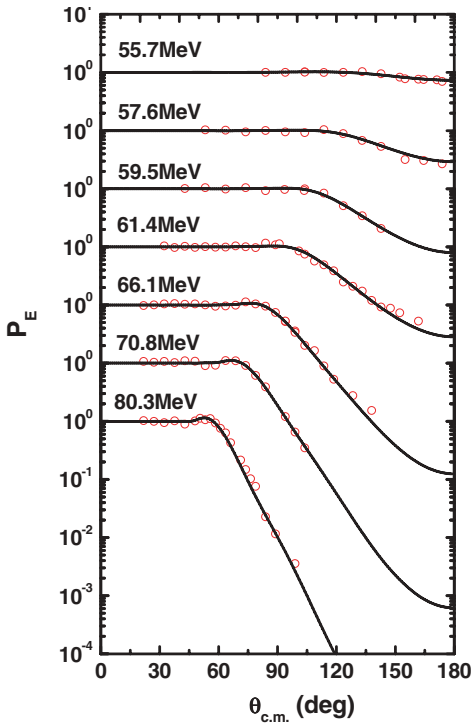

FIG. 5. (Color online) Ratios of the elastic scattering cross sections to the Rutherford cross section calculated with our final dispersive optical potentials are shown in comparison with the experimental data. The data are taken from Ref. [12].

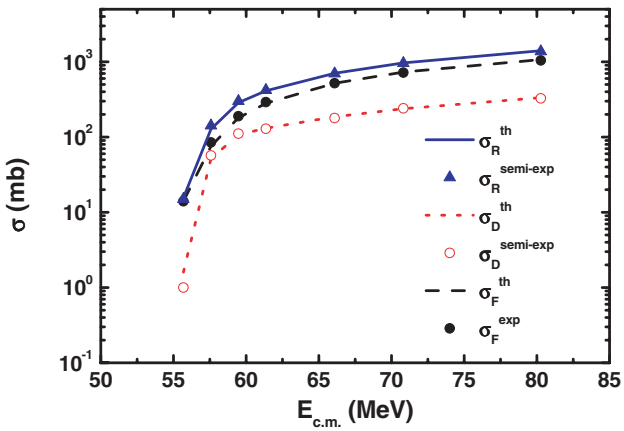

FIG. 6. (Color online) DR and fusion cross sections calculated with our final dispersive optical potential are shown in comparison with the experimental data. $\sigma_D^{\rm semi-exp}$ denoted by the open circles are obtained as described in Sec. III. The fusion data are from Ref. [13].

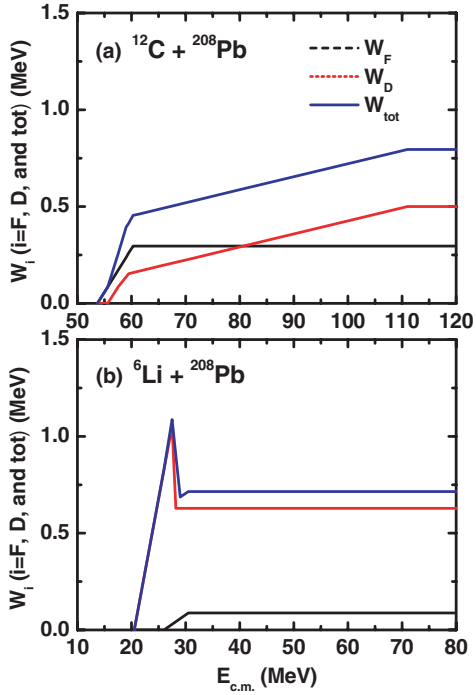

FIG. 7. (Color online) The values of the fusion, DR, and total imaginary potential, $W_F(r, E)$, $W_D(r, E)$ and $W_{\rm tot}(r, E)$, respectively, (a) at $r = R_{sa} = 12.3$ fm for ^{12}C+^{208}Pb and (b) at $r = R_{sa} = 12.4$ fm for ^{6}Li+^{208}Pb.

F. Discussions

As already remarked in Sec. IV D, the real and the imaginary parts of both DR and fusion polarization potentials determined from the present χ^2 analyses satisfy the dispersion relation [10,11] separately. We showed in Ref. [1] that for the case of the ^{6}Li+^{208}Pb system the threshold anomaly as was observed in heavy ion collisions involving strongly bound projectiles [24–26] were distinctly seen only in the fusion potential; the values of the DR potential changes with energy much more slowly than those of the fusion potential. Now, for the present case of ^{12}C+^{208}Pb, Fig. 4 shows that the values of $W_D(E)$ are smaller than those of $W_F(E)$ by about ten times. However, a somewhat different picture emerges if one plots the values of the imaginary parts of the DR and fusion potentials at a strong absorption radius $r = R_{sa}$, i.e., $W_D(R_{sa}, E)$ and $W_F(R_{sa}, E)$, respectively. In Fig. 7(a), plotted are the values of $W_D(R_{sa}, E)$ and $W_F(R_{sa}, E)$, together with the sum, $W_{\rm tot}(R_{sa}, E)$, assuming $R_{sa} = 12.3$ fm. In Fig. 7(b), we also show for the sake of comparison the values of $W_D(R_{sa}, E)$ and $W_F(R_{sa}, E)$ at $r = R_{sa} = 12.4$ fm for the ^{6}Li+^{208}Pb system obtained with the dispersive potentials of Ref. [1].

It can be seen in Fig. 7(a) that the magnitudes of $W_D(R_{sa}, E)$ are now comparable with those of $W_F(R_{sa}, E)$ and that $W_D(R_{sa}, E)$ increases as much rapidly as $W_F(R_{sa}, E)$ does with almost the same threshold energies. We can also see that $W_F(R_{sa}, E)$ is larger than $W_D(R_{sa}, E)$ around the Coulomb barrier energy for the ^{12}C+^{208}Pb system, which is consistent with the ratio R_F shown in Fig. 2. The sum $W_{\rm tot}(R_{sa}, E)$ of $W_D(R_{sa}, E)$ and $W_F(R_{sa}, E)$ increases rapidly as typically observed for strongly bound projectiles [24–26]. In contrast to the above features of $W_{\rm tot}(R_{sa}, E)$, $W_D(R_{sa}, E)$, and $W_F(R_{sa}, E)$ for the ^{12}C+^{208}Pb system, those of the ^{6}Li+^{208}Pb system are very different; first of all, as seen in Fig. 7(b), $E^{\rm exp}_{0,D} \ll E^{\rm exp}_{0,F}$ and the total $W_{\rm tot}(R_{sa}, E)$ is dominated by $W_D(R_{sa}, E)$, which is again consistent with the ratio R_F in Fig. 2, and thus $W_{\rm tot}(R_{sa}, E) \simeq W_D(R_{sa}, E)$ over the whole energy range considered.

V. CONCLUSIONS

Simultaneous χ^2 analyses are made for the elastic scattering and fusion cross section data for the ^{12}C+^{208}Pb system at near-Coulomb-barrier energies based on the extended optical model approach in which the polarization potential is decomposed into direct reaction (DR) and fusion parts. Use is made of the double folding potential as a bare potential. It is found that the experimental elastic scattering and fusion data are well reproduced without introducing any normalization factor for the double folding potential and also that both DR and fusion parts of the polarization potential determined from the χ^2 analyses satisfy separately the dispersion relation. Moreover, it is found that the imaginary parts of both fusion and DR potentials at the strong absorption radius show rapid energy variation around the Coulomb barrier energy which is typical for tightly bound projectiles [24–26]. The results are compared with those for the ^{6}Li+^{208}Pb system involving a loosely bound projectile ^{6}Li.

ACKNOWLEDGMENTS

The work was supported in part by the Korea Research Foundation Grant funded by the Korean Government (MOEHRD)(KRF-2006-214-C00014) and the Korea Science and Engineering Foundation grant funded by the Korean Government (MOST) (No. M20608520001-07B0852-00110).

[1] W. Y. So, T. Udagawa, K. S. Kim, S. W. Hong, and B. T. Kim, Phys. Rev. C **75**, 024610 (2007).
[2] W. Y. So, T. Udagawa, K. S. Kim, S. W. Hong, and B. T. Kim, Phys. Rev. C **76**, 024613 (2007).
[3] W. Y. So, T. Udagawa, K. S. Kim, S. W. Hong, and B. T. Kim, to be submitted.
[4] T. Udagawa, B. T. Kim, and T. Tamura, Phys. Rev. C **32**, 124 (1985); T. Udagawa and T. Tamura, *ibid.* **29**, 1922 (1984).
[5] S.-W. Hong, T. Udagawa, and T. Tamura, Nucl. Phys. **A491**, 492 (1989).
[6] T. Udagawa, T. Tamura, and B. T. Kim, Phys. Rev. C **39**, 1840 (1989); B. T. Kim, M. Naito, and T. Udagawa, Phys. Lett. **B237**, 19 (1990).
[7] G. R. Satchler and W. G. Love, Phys. Rep. **55**, 183 (1979).
[8] Y. Sakuragi, Phys. Rev. C **35**, 2161 (1987).
[9] N. Keeley and K. Rusek, Phys. Lett. **B427**, 1 (1998).

[10] C. C. Mahaux, H. Ngô, and G. R. Satchler, Nucl. Phys. **A449**, 354 (1986); **A456**, 134 (1986).
[11] M. A. Nagarajan, C. C. Mahaux, and G. R. Satchler, Phys. Rev. Lett. **54**, 1136 (1985).
[12] S. Santra, P. Singh, S. Kailas, A. Chatterjee, A. Shrivastava, and K. Mahata, Phys. Rev. C **64**, 024602 (2001).
[13] A. Mukherjee, D. J. Hinde, M. Dasgupta, K. Hagino, J. O. Newton, and R. D. Butt, Phys. Rev. C **75**, 044608 (2007).
[14] W. Y. So, S. W. Hong, B. T. Kim, and T. Udagawa, Phys. Rev. C **69**, 064606 (2004).
[15] N. Keeley, S. J. Bennett, N. M. Clarke, B. R. Fulton, G. Tungate, P. V. Drumm, M. A. Nagarajan, and J. S. Lilly, Nucl. Phys. **A571**, 326 (1994).
[16] J. J. Kolata, V. Guimarães, D. Peterson, P. Santi, R. White-Stevens, P. A. DeYoung, G. F. Peaslee, B. Hughey, B. Atalla, M. Kern, P. L. Jolivette, J. A. Zimmerman, M. Y. Lee, F. D. Becchetti, E. F. Aguilera, E. Martinez-Quiroz, and J. D. Hinnefeld, Phys. Rev. Lett. **81**, 4580 (1998).
[17] W. G. Love, T. Terasawa, and G. R. Satchler, Nucl. Phys. **A291**, 183 (1977).
[18] B. T. Kim, W. Y. So, S. W. Hong, and T. Udagawa, Phys. Rev. C **65**, 044607 (2002).
[19] M. S. Hussein, Phys. Rev. C **30**, 1962 (1984).
[20] C. W. De Jager, H. DeVries, and C. DeVries, At. Data Nucl. Data Tables **14**, 479 (1974).
[21] J. Cook, Comput. Phys. Commun. **25**, 125 (1982).
[22] P. H. Stelson, Phys. Lett. **B205**, 190 (1988); P. H. Stelson, H. J. Kim, M. Beckerman, D. Shapira, and R. L. Robinson, Phys. Rev. C **41**, 1584 (1990).
[23] B. T. Kim, W. Y. So, S. W. Hong, and T. Udagawa, Phys. Rev. C **65**, 044616 (2002).
[24] A. Baeza, B. Bilwes, R. Bilwes, J. Diaz, and J. L. Ferrero, Nucl. Phys. **A419**, 412 (1984).
[25] J. S. Lilley, B. R. Fulton, M. A. Nagarajan, I. J. Thompson, and D. W. Banes, Phys. Lett. **B151**, 181 (1985).
[26] B. R. Fulton, D. W. Banes, J. S. Lilley, M. A. Nagarajan, and I. J. Thompson, Phys. Lett. **B162**, 55 (1985).